Journal of Applied Electrochemistry (2022) 52:1761–1771
https://doi.org/10.1007/s10800-022-01744-4

RESEARCH ARTICLE

Molecularly imprinted copolymer/reduced graphene oxide for the electrochemical detection of herbicide propachlor

Reda Elshafey[1] · **Abd-Elgawad Radi**[1]

Received: 28 March 2022 / Accepted: 6 August 2022 / Published online: 27 August 2022

Abstract

The toxicity of propachlor (PROP) with its chloroacetanilide members is reported. Rapid and sensitive detection of PROP is critical for ecotoxicity evaluation and the removal process. A novel voltammetric sensor is developed based on imprinted poly (o-phenylene diamine-co-pyrrole) (o-PD-co-Py) and electrochemically reduced graphene oxide (ERGO) to detect PROP at a trace level. The use of ERGO provides a high density of imprinted cavities for better sensitivity. The imprinted layer of poly (o-PD-co-Py) improves the selectivity of the sensor. The electrode modification was characterized by scanning electron microscopy and electrochemical approaches. The working parameters of the sensor were investigated and optimized. The redox behavior of an external probe of $[Fe(CN)_6]^{3-/4-}$ was recorded as the sensor signal for PROP selective binding. The proposed sensor presented wide linear responses to logarithmic PROP concentrations from 0.1 pM to 0.1 µM with a LOD of 0.08 pM. The sensor's selectivity against some interference was demonstrated. This sensor was applied successfully to detect PROP in spiked water (lake and tap), red tea, and soil samples with good recoveries and reasonable RSD % values.

Graphical abstract

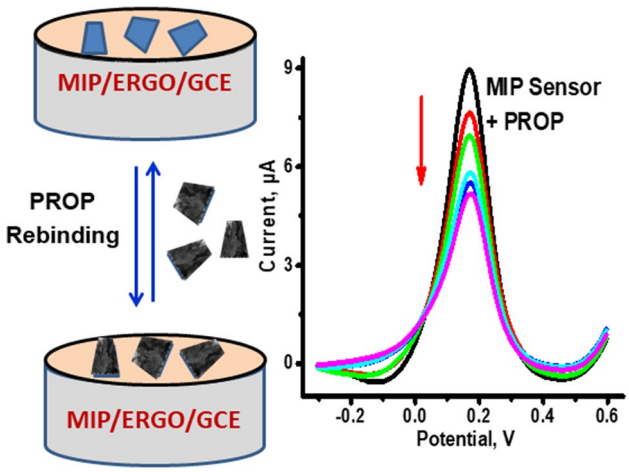

Keywords Propachlor · Reduced graphene oxide · Pyrrole · *o*-phenylene diamine · Voltammetry · Imprinted polymer

1 Introduction

Chloroacetanilide herbicides are widely used as pre-emergence for weed control in corn and soybeans. These herbicides and their metabolites have been frequently detected in groundwater and surface waters [1–3]. Propachlor [PROP, (2-chloro-N-(1-methylethyl)-N-phenylacetamide)] is one of

✉ Abd-Elgawad Radi
abdradi@du.edu.eg

[1] Faculty of Science, Department of Chemistry, Damietta University, Damietta 34517, Egypt

the most used chloroacetanilide herbicides after alachlor and metolachlor in European countries and China [4, 5]. PROP is applied to limit the broad-leaved and grass weeds in corn, green peas, soybeans, and strawberries [6] by blocking protein synthesis. PROP was registered as a pesticide in the US in 1964; however, in 2001, it was added as a carcinogen to California's Proposition 65 list [7]. According to EPA Agency, PROP was classified as a likely human carcinogen.

PROP is highly toxic for some aquatic organisms [8] in addition to the moderate toxicity to birds. According to laboratory animal studies, PROP is classified as a toxicity category I (severe) for eye irritation potential and dermal sensitizer. PROP showed cytotoxicity in rats and human cell lines based on the studies of chloroacetanilide herbicides [9]. The toxicity effects of PROP on humans and the environment required its determination at the trace level.

The degradation and the removal of PROP from food and environmental samples have been reported [6, 10–13]. The sensitive determination of PROP levels is an essential prerequisite for efficient degradation and removal conditions. The current detection approaches for analyzing PROP are not sensitive to tracing its low level in environmental samples. The detection of PROP individually is rarely developed; instead, it has been monitored with other chloroacetanilides members or pesticides. Gas chromatography (GC) coupled with mass spectrometry (MS) or tandem mass methods were developed to detect PROP, mostly with other chloroacetanilide herbicides [14–19]. In more recent reports, liquid chromatography (LC) [20], LC–MS/MS [21], and ultra-high-performance liquid chromatography coupled with quadrupole time-of-flight mass spectrometry (UPLC-QTOF-MS) [22] have been applied for PROP determination with other pesticides in soil, hair, and tea samples, respectively.

Despite the popularity of electrochemical sensors for pesticides detection [23–26], no electrochemical assays were reported for PROP. This study develops a molecularly imprinted copolymer (o-phenylene diamine co-pyrrole) for the PROP voltammetric sensing based on electrochemically reduced graphene oxide (ERGO) modified glassy carbon electrode.

Molecularly imprinted polymers (MIPs) have been extensively employed in sensing and separation purposes, owning their specific recognition properties. The bulk polymerization of the MIP encountered limits for electrochemical applications. The simplicity and accessibility to control MIP thickness are advantages of surface-generated MIPs. Several reports have used a single functional monomer for MIP electrosynthesis; however, few have used pyrrole and o-phenylene diamine (o-PD) [27, 28]. MIP formation using two monomers generates the diversity of the imprinted cavities of modulated affinity and improves sensor sensitivity and selectivity. Since the sensor's sensitivity is influenced by the density of the recognition elements on the electrode [29, 30], the nanomaterials integration into the electrode would enhance the sensitivity. The modification of electrode with nanostructures also improves the conductivity and facilitate the electron transfer process.

As reported, MIPs synthesized on nanostructured surfaces may have up to 15 times more imprinted cavities compared to those prepared on non-modified surfaces [31, 32]. Reduced graphene oxide (RGO) has attracted researchers' attention in electrochemical sensing applications [33–35] due to its excellent electrical conductivity, high electroactive area, and low cost, in particular for those based on the molecularly imprinted polymers [36–39]. Electrochemically reduced graphene oxide (ERGO) exhibited high conductivity and surface area than GO; thus, it is suitable as electrode material in electron transfer reactions. We use MIP as a specific receptor and ERGO as an electrode modifier to develop an ultrasensitive PROP electrochemical sensor. The sensor combines the specificity and pre-concentration capability of the MIP receptor with the high surface area of ERGO. To the best of our knowledge, no MIP-ERGO-based sensor for PROP has been reported. The sensing parameters that influenced its sensitivity and selectivity were investigated. These are the ratio of the pyrrole/o-PD monomers, electropolymerisation cycles, the medium solution used for the MIP formation, template removal time, and the recognition time. The sensor selectivity was demonstrated against the commonly used pesticides alachlor, carbendazim, and dimethoate in addition to some ions. Finally, the actual application of the sensor was shown in lake and tap water samples.

2 Experimental

2.1 Reagents and apparatus

Propachlor, alachlor, pyrrole, o-phenylene diamine, potassium ferricyanide, and potassium chloride were purchased from Sigma-Aldrich, USA. All other chemicals were supplied in analytical grade and used as received. Acetate buffer solution of pH 5.2, 0.2 M (ABS) was prepared using acetic acid and sodium acetate in proper amounts. Phosphate buffer saline (PBS), pH 7.4 (0.1 M) was prepared using disodium hydrogen phosphate, sodium dihydrogen phosphate, and potassium chloride.

The pH meter (Mettler Toledo MP225, Switzerland) was used to read the pH values and adjust the pH of buffers. Electrochemical measurements were performed using a PGSTAT 302 N Autolab potentiostat/ galvanostat (Eco-Chemie, The Netherlands) controlled by Nova 1.11 software. A conventional electrochemical cell of three electrodes is used: Ag/AgCl (3 M KCl) used as a reference electrode, a platinum wire employed as the auxiliary electrode, and a glassy carbon electrode (GCE, diameter: 3.0 mm) modified

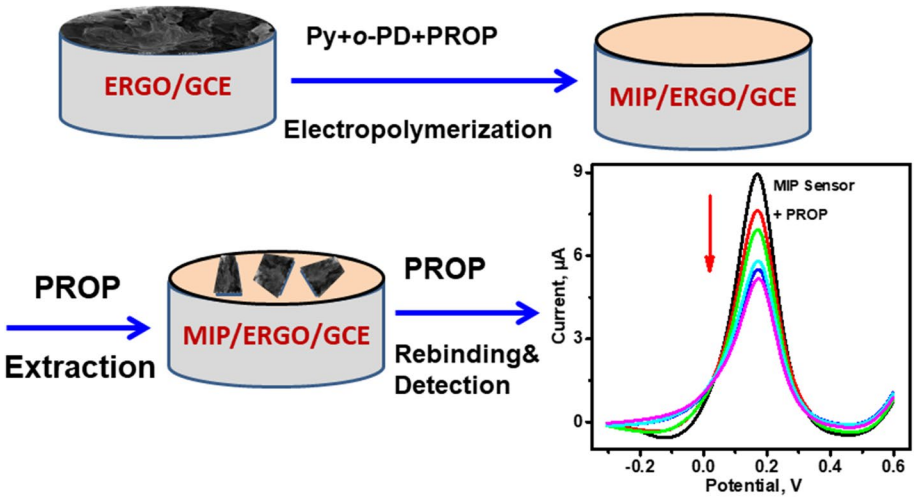

Scheme 1 Representation of the MIP formation on ERGO/GCE surface, the recognition, and the detection process of PROP

with ERGO and MIP as working electrode. All measurements were performed in triplicate at room temperature.

2.2 Fabrication of MIP/ERGO/GCE sensor

The GCE was first polished to a mirror-like surface with 0.3 µm alumina, washed with distilled water, and then subjected to ultrasonication for 3 min to remove adsorbed solid particles on its surface. Graphene oxide (GO) was prepared by a modified Hummers' method [40] and used to modify the GCE. 10.0 µL of GO aqueous suspension (5 mg/mL) was cast on the GCE surface to obtain GO/GCE and left to dry in the air at room temperature. The ERGO-modified electrode (ERGO/GCE) was made by sweeping the GO/GCE electrode's potential between 0.2 and − 1.2 V vs. Ag /AgCl at a scan rate of 100 mV s^{-1} for 20 cycles in phosphate buffer pH 7.2 (0.2 M). For the electrosynthesis of the molecularly imprinted poly(o-PD-co-pyrrole) film, the ERGO/GCE electrode was immersed in an acetate buffer solution pH 5.2 (0.2 M) containing the mole ratio of (o-PD: Py: PROP), (2: 2: 1) (the optimal monomers to PROP ratio).

Cyclic voltammetry was applied in a potential range of 0.0 to 1.1 V at 100 mV s^{-1} for 15 consecutive cycles. Then the PPY-PoPD/ERGO/GCE electrode was immersed in methanol-acetic acid solution (9:1; v:v) for 15 min to leach out the PROP molecules. Under the same conditions, the non-imprinted electrode (NIP-ERGO/GCE) was synthesized without PROP. The stepwise elaboration of the MIP-modified ERGO-based sensor is shown in Scheme 1.

2.3 Sensor characterization

The electrochemical characterization of the electrode was performed by cyclic voltammetry (CV), differential pulse voltammetry (DPV), and electrochemical impedance spectroscopy (EIS). The CV measurements were performed in a potential range of − 0.40 to 0.80 V at 50 mV s^{-1}. The optimization of DPV conditions was carried out. The effect of step potential (5 mV& 6 mV) and the modulation amplitude (25 mV and 50 mV) on the DP voltammograms of the redox probe was investigated. A well-defined DPV peak with high intensity was recorded at a step potential and amplitude of 5 mV and 25 mV, respectively. Therefore, the potential range of − 0.25 to 0.60 V at a scan rate of 10.0 mV s^{-1}, a step potential of 5.0 mV, and modulation amplitude of 25 mV were applied to conduct the DPV experiments during the MIP sensor formation and application.

The EIS measurements were performed using a fixed potential of 0.20 V, a potential amplitude of 5 mV, and a frequency range of 0.1 µHz to 0.01 Hz. All electrochemical measurements were performed from a solution of 0.1 M KCl containing 2.0 mM $[Fe(CN)_6]^{3-/4-}$ as an electrochemical probe. The morphological characterization of GCE modified with GO and ERGO was performed by scanning electron microscopy using a JEOL microscope, model JSM 6510 lv.

2.4 Electroanalytical measurements

For the sensor rebinding to PROP, the sensor was placed in PBS, pH 7.4 solution containing a series of PROP concentrations for 5 min. The change in the MIP electrode upon the rebinding of PROP was monitored by recording the DPV current from 0.1 M KCl containing 2.0 mM $[Fe(CN)_6]^{3-/4-}$ probe. The MIP/ERGO/GCE sensor selectivity was investigated by using some common potential pesticides such as herbicide alachlor (ALA), fungicide carbendazim (CBZ), an insecticide dimethoate (DMT) in addition to some inorganic ions of Na^+, K^+, SO_4^{2-}, and Cl^-. The sensor is incubated in each pesticide at 0.01 nM, 0.1 nM, and 1.0 nM, and sensor responses were recorded and compared to the PROP binding. Inorganic ions were used at 1.0 mM.

2.5 Determination of PROP in real samples

The water (tap and lake), red tea, and soil samples were employed for the MIP sensor testing. The lake water and soil samples are obtained from a nearby lake and a garden located in Damietta city, Egypt. The tea sample was supplied from a local market. For the water samples, PROP was spiked in different amounts. While for soil and tea samples, the extraction process was made before the spiking of PROP. For the soil sample, the PROP of various amounts is added separately to 0.1 gm sieved soil, then subjected to vertex for 5 min and incubated for 1 h. The supernatant of PROP was obtained by centrifugation. For the tea sample, 0.5 g was added to 4 mL distilled water, after vertex for 5 min and incubation for 30 min, the acetonitrile is added and vertex for 5 min. The obtained extract is used to prepare each PROP concentration by keeping its composition to the buffer PBS, pH 7 constant (filtrate: PBS; 20:80 v:v). Each treated sample (water, tea, and soil) was subjected to DPV measurements, and the sensor signals were used to calculate the added PROP using the standard curve. The recovered values were evaluated with the relative standard deviation.

3 Results and discussion

3.1 Sensor characterization

The GCE modification with GO and ERGO was investigated by conducting the CV and EIS from a solution of 0.1 M KCl containing 2.0 mM $[Fe(CN)_6]^{3-/4-}$ probe. Figure 1a shows the characteristic quasi-reversible electrochemical behavior of $[Fe(CN)_6]^{3-/4-}$ on the GCE (curve a).

Following the electrode modification with GO (curve b), the peak current decreased with an increase in the peak separation. However, after the electrochemical reduction of some oxygen-containing groups to form ERGO/GCE, the peak current was enhanced (13.38 µA) with a drop in peak separation (ΔE_p of 83.1 mV).

The formation of GO and ERGO-modified electrodes was also characterized by EIS (Fig. 1b). A large semi-circle radius was measured (R_{et} = 20.6 KΩ) from GO/GCE to bare GCE (R_{ct} = 284 Ω); (Fig. 1b, curves b, a) this indicates that the use of GO retards the electron transfer process of the redox probe at the electrode interface. A significant drop in the R_{et} value (6.24 Ω, Fig. 1b, curve c) was recorded from the ERGO/GCE. Such decrease may be originated from the low density of negatively charged oxygen-containing groups (after the electrochemical reduction of GO). The repulsion between the ERGO electrode surface and the negatively charged redox probe decreases and facilitates the electron transfer process. These results were well compared to the CV results in Fig. 1a.

The catalytic activity of ERGO [36, 39] and the enhanced electrode effective area due to the presence of ERGO may be the reasons for that behavior. Such surface area was calculated from the Randles–Sevcik equation at various scan rate values in a solution of 0.1 M KCl containing 1.0 mM $K_3[Fe(CN)_6]$ and compared to bare GCE and GO/GCE. A 1.19 cm^2 value was calculated for ERGO/GCE, which is 1.13-fold of GCE (1.05 cm^2) and 2.42 times to GO/GCE (0.49 cm^2). The Randles equivalent circuit (Fig. 1b, inset) was used for fitting the experimental data.

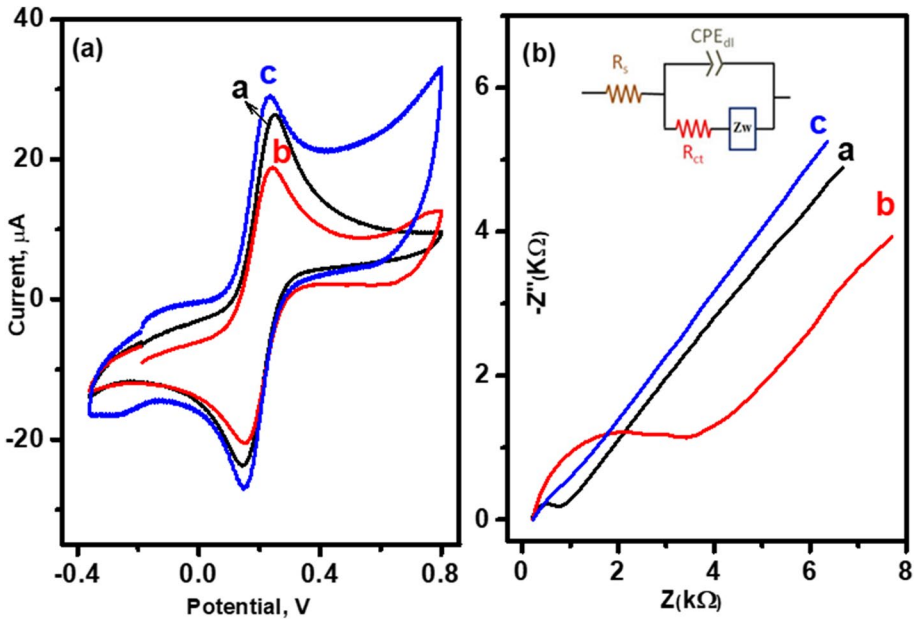

Fig. 1 **a**, **b** CVs and EIS for the characterization of GCE modifications: (a) bare GCE, (b) GO/GCE, (c) ERGO/GCE conducted from 2.0 mM $[Fe(CN)_6]^{3-/4-}$ in 0.1 M KCl. Inset of (**b**) is the equivalent circuit used for Nyquist plot fitting

At high frequencies, the semi-circle region is related to the charge-transfer resistance (R_{ct}) at the electrode-solution interface and the constant phase element (CPE). While the linear part of the diagram was recorded at low frequencies, the Warburg impedance (W) was measured, which related to the diffusion of the redox probe to the electrode surface.

The molecularly imprinted poly (*o*-PD-co-Py) film was electrosynthesized on the ERGO/GCE surface using ABS; pH 5; 0.2 M containing 2.0 mM of *o*-PD, and Py monomers in the presence of PROP at 1.0 mM as a template. Figure 2a shows the voltammograms obtained during the electropolymerisation process; three irreversible peaks were observed. The oxidation peaks at 0.28 V and 0.52 V were characteristic of *o*-PD, and the broad one at about 0.72 V was attributed to the oxidation of Py. No peaks appear from the PROP; it is an electro-inactive herbicide. These oxidation peaks decreased after the first cycle, indicating the formation of a PPy-POD non-conductive polymer film on the ERGO/GCE surface (Fig. 2a, b). No significant differences are observed between the voltammograms obtained in the absence (NIP/ERGO/GCE) and presence of PROP; this shows that PROP does not present any oxidation or reduction in the potential range used for electropolymerisation. However, more charge density is consumed in NIP/ERGO/GCE (Fig. 2b).

Following the MIP formation on the ERGO/GCE electrode, its properties were characterized by conducting the DPVs and EIS from the redox probe. A similar drop in peak current was measured from MIP/ERGO/GCE and NIP/ERGO/GCE electrodes (Fig. 3a curves a and d). The Nyquist

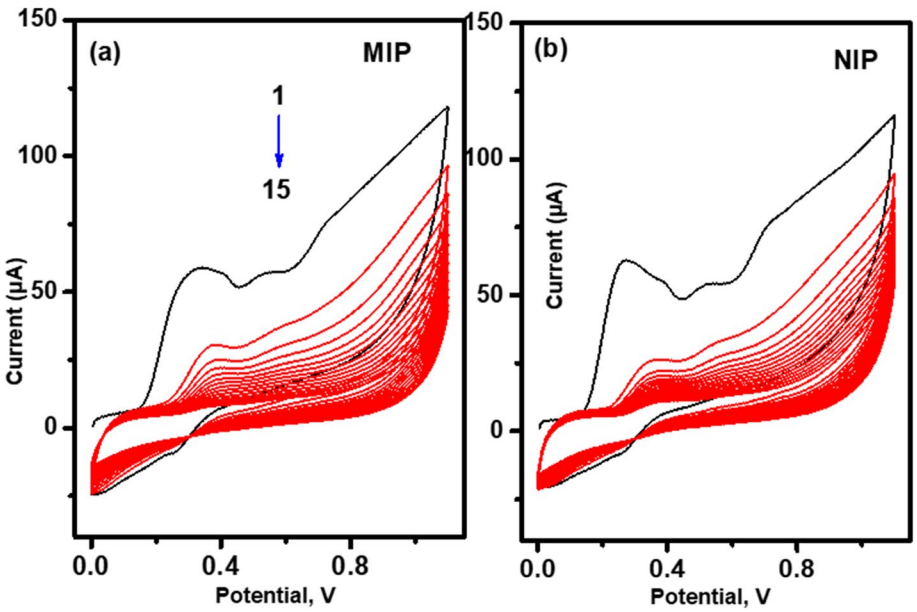

Fig. 2 **a**, **b** Electrosynthesis of MIP and NIP onto ERGO/GCE in ABS (0.2 M), pH 5.2 solution containing 2.0 mM o-PD and pyrrole with and without 1.0 mM PROP, respectively by CV with a scan rate of 50 mV s^{-1} between − 0.2 and 1.1 V vs. Ag/AgCl (3 M KCl) ref. electrode for 15 cycles

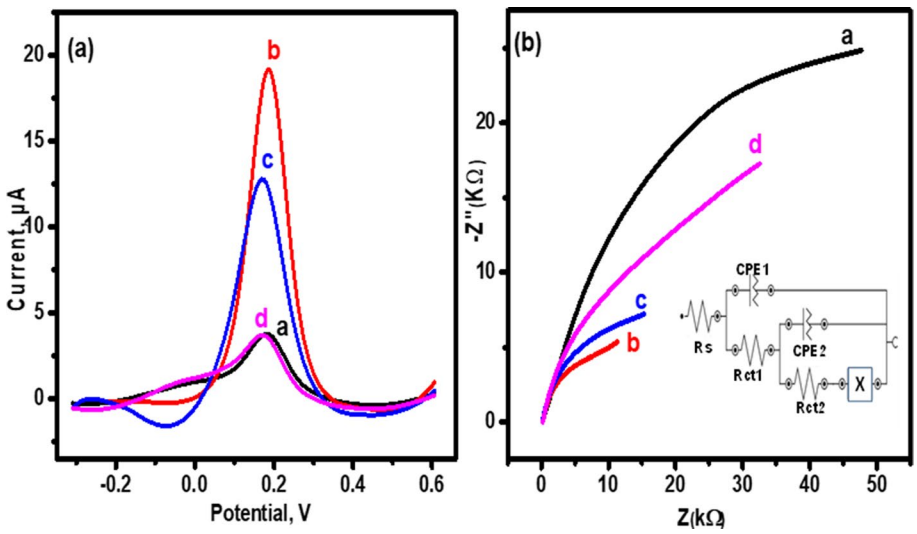

Fig. 3 **a** DPVs and **b** Nyquist diagrams conducted from 0.1 M KCl solution containing 2.0 mM $[Fe(CN)_6]^{3-/4-}$ for: **a** ERGO/GCE after electropolymerisation; **b** MIP/ERGO/GCE after the removal of PROP template using methanol-acetic acid solution (9:1; v:v) for 15 min; **c** MIP/ERGO/GCE after rebinding process for 5 min in PBS solution containing 0.1 pM PROP, and **d** NIP/ERGO/GCE. Inset: Equivalent circuit used in the experimental EIS fitting

plots were consistent with the DPV behavior (Fig. 3b, curves a and d). A large semi-circle radius for MIP to the NIP electrode was observed (9.51 KΩ vs. 5.88 KΩ), indicating the formation of a non-conductive polymer film in the presence of PROP (Fig. 3b, curves a, d). The non-conductive poly (*o-PD*-co-Py) imprinted PROP layer blocked the electrode surface and impeded the redox process of the redox probe, resulting in the current drop or R_{et} increase. Upon extracting the PROP template using methanol/acetic acid solution (9:1; v: v), a typical DPV peak from the MIP-free PROP electrode is measured (Fig. 3a, curve b) due to the formation of cavities specific to the PROP molecules. Such cavities facilitate the accessibility of the redox marker to the electrode surface and undergo electron transfer. The measured drop in R_{et} of 2.3 KΩ (Fig. 3b, curve b) supported the increase of DPV peak current (Fig. 3a, curve b), both evidenced the successful removal of the PROP from the MIP polymer matrix. At the rebinding of 0.1 pM PROP to the MIP-ERGO/GCE sensor, a drop in DPV current was observed (Fig. 3a, curve c). The recognition of PROP molecules to the imprinted cavities (complementarity to the shape and size of PROP) resulted in blocking the transfer of the $[Fe(CN)_6]^{3-/4-}$ to the electrode surface. An increase of R_{et} (5.84 KΩ) was measured (Fig. 3b, curve c) which is consistent with the DPV results.

The equivalent circuit (inset of Fig. 0.3b) was used to analyze and fit the experimental data. It contains a solution resistance (Rs), two constant phase elements (CPE1, CPE2) in parallel to two charge-transfer resistances (Rct_1, Rct_2), and an element X. At the MIP/ERGO/GEC and NIP/ERGO/GCE (Fig. 0.3b, curves a and d), the X element may represent a tangent-hyperbolic function (T) which describes a finite-length diffusion circuit. Based on this, a thin non-conductive layer represents either NIP or MIP on a conductive electrode (ERGO/GCE) and blocks the diffusion of the species in solution [36, 41]. This clearly describes the system under study where poly(o-PD-co-Py) or poly(o-PD-co-Py-PROP) films immobilized on the ERGO/GCE block the surface and impede the diffusion rate of the redox probe. While at the surface of MIP-free PROP and after rebinding of PROP (curves b and c), the X element assumes the presence of a porous electrode (cavities are formed and still present after rebinding to some extent) [36, 42]. This element also interprets the MIP sensor since the imprinted cavities on the polymer matrix are considered porous.

To verify that the signal change upon binding of PROP was specific, the same measurements were performed using NIP-ERGO/GCE electrode (non-imprinted polymer). We challenged the MIP/ ERGO/GCE and NIP/ ERGO/GCE electrodes to bind PROP (100 pM and 1 nM). The change in the sensor signal recorded from the MIP and NIP modified ERGO/GCE electrodes were compared and used to calculate the imprinted factor:

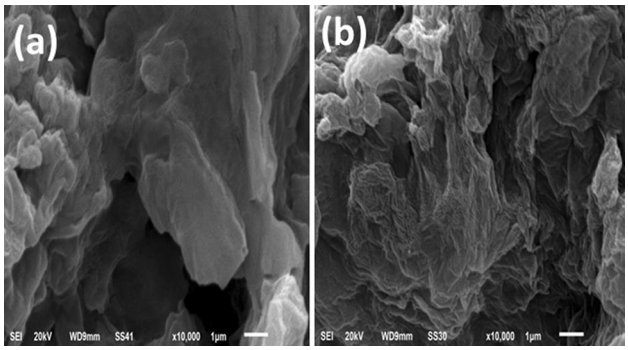

Fig. 4 SEM images for **a** GO/GCE, and **b** ERGO/GCE

$$IF = \frac{\Delta i/i_0\%(MIP + PROP)}{\Delta i/i_0\%(NIP + PROP)}$$

where Δi_0 is the difference between i_0 and i (the current of the redox probe that is recorded from the MIP and NIP electrodes before and after the binding to PROP, respectively). The IF of 4.61 and 4.97, respectively, were calculated from *o-PD* : Py: PROP at the ratio of (2:2:1). Such findings evidenced that the change observed is induced by the specific binding of PROP to the MIP sensor and not by non-specific adsorption of the PROP onto the NIP/ERGO/GCE.

3.2 Surface characterization of modified electrodes

The morphological properties of the electrode modifications were conducted by capturing the SEM images. Figure 4a shows the GCE surface modified with GO, flakes-like sheets were observed, which is typically characteristic to GO. More wrinkle sheets of high transparency were observed after the electrochemical reduction of GO to obtain ERGO (Fig. 4b), indicating the increase of the electroactive area of this electrode.

3.3 Optimization of MIP/ERGO/GCE sensor

Some experimental conditions are investigated for efficient MIP sensor analytical performance. The sensor signals ($\Delta i/i_0\%$) were compared for each parameter, evaluated, and used to determine the optimal conditions. The density of imprinted cavities formed is related to the functional monomers (o-PD and Py) ratio and the template molecule (PROP). We kept the target concentration at 1 mM, while the proportion of Py to *o*-PD is interchanged (Fig. 5a). A decrease in the sensor responses was observed at the mole ratio values except for 2:2:1 due to the formation of a low or high density of cavities in MIP sensors. Similar signals were recorded from the NIP electrode, and the MIP formed with o-PD, demonstrating the crucial role of the Py in the formation of highly selective MIP film (Fig. 5a). Thus, the ratio of 2:2:1

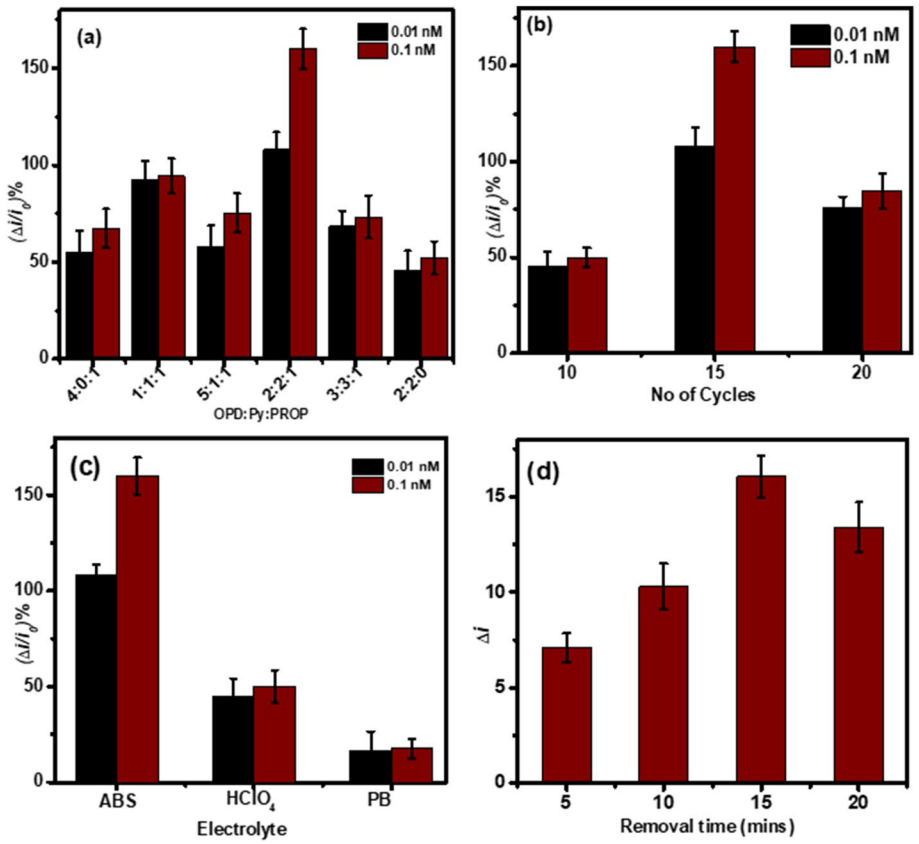

Fig. 5 Comparison of MIP/ERGO/GCE sensor responses ($\Delta i/i\%$) at the binding of 0.01 and 0.1 nM PROP for **a** different mole ratio of monomers of Py and *o-PD* to PROP template, **b** a various number of electropolymerisation cycles, and **c** different electrolyte solutions used for MIP electrosynthesis, **d** influence of the immersion time of MIP/ERGO/GCE in methanol-acetic acid (9:1; v:v) on its response (Δi) for PROP removal. The error bars represent the SD of three measurements

(2 mM O-PD, 2 mM Py, and 1 mM PROP) was chosen as the optimal molar ratio for subsequent studies.

The thickness of the MIP film is critically affected by the number of cycles employed in the electropolymerisation process. A decrease in the sensor responses was observed at the voltammetric cycles rather than 15 because of the formation of thick or thin MIP layers; this is probably due to the inefficient removal process and instability of the MIP sensor at a lower molar ratio. (Fig. 5b). Thus, 15 cycles were chosen as suitable for the electropolymerisation of the molecularly imprinted poly(o-PD-co-Py) film on the ERGO/GCE electrode. It is well known that the pH of an electrolyte used in the electrosynthesis of MIP has affected the generation of the intermediates responsible for forming imprinted polymer chains. Acetate buffer (ABS) pH 5.0 is usually used in the electropolymerisation of *o-PD*; however, a neutral pH value is also employed, such as phosphate buffer (PB). As pyrrole is used as a functional co-monomer, perchloric acid will be tested.

Thus, $HClO_4$, acetate buffer (pH 5.0), and PB (pH 7.0) were used as electrolyte solutions for electropolymerisation. The sensor response increases by raising the pH value and recording the highest from the ABS; pH 5 (Fig. 5c). At acidic or neutral pH values, i.e., $HClO_4$ and PB, the sensor response decreases due to the imperfect polymerization of Py and o-PD (deficient radicals formed). Therefore, the ABS at pH of 5.0 was chosen as the ideal for conducting the electropolymerisation process.

The template removal is a crucial factor in controlling the density of imprinted cavities. Organic solvents are widely applied since they do not affect the stability of the polymer matrix [43]. In this method, the swelling of the polymer matrix occurred, which weakens the interactions between the poly(*o-PD*-co-Py) film and the PROP molecules, releasing the template and forming the imprinted cavities. Methanol-acetic acid solutions with various volume ratios were used to extract PROP molecules from the imprinted matrix; at the ratio of (9:1; v:v), highly efficient imprinted cavities are formed.

Thus, the DPV signal of MIP/ERGO/GCE was measured before and after immersing in methanol-acetic acid (9:1; v:v) for 5, 10, 15, and 20 min (Fig. 5d). The (Δi) refers to the difference between the redox probe peak current recorded from the MIP electrode and after its incubating in methanol-acetic acid solution at various time intervals. As noted in (Fig. 5d), when the removal time increases, the Δi increases with a maximum value at 15 min, while a drop in such value was obtained at 20 min. The polymer swelling may lead to the deformation and blockage of the imprinted cavities, which prevents the redox probe from reaching the electrode surface. Thus the immersion of the sensor in methanol-acetic

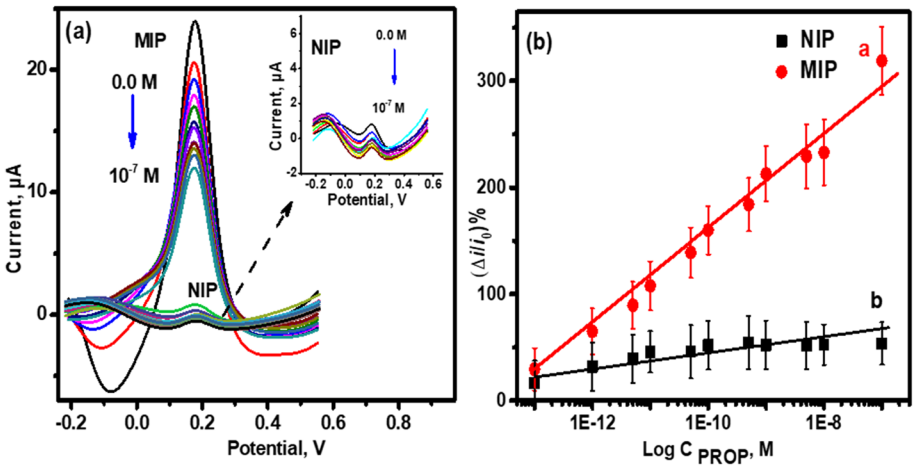

Fig. 6 **a** DPVs of MIP/RGO/GCE and NIP/ERGO/GCE conducted from 2.0 mM $[Fe(CN)_6]^{3-/4-}$ in 0.1 M KCl after incubation in PROP of different concentrations (0.1 pM to 0.1 µM) in 0.2 M PBS for 5 min. **b** The calibration curves corresponding to MIP/ERGO/GCE (**a**) and NIP/ERGO/GCE (**b**) responses related to Log C_{PROP}. Error bars are the SD of three independent measurements

acid (9:1; v:v) for 15 min was optimal for removing PROP molecules from the polymer matrix.

The equilibrium time required to rebound PROP molecules to the imprinted cavities affects the sensor's sensitivity. Following the extraction of the template molecule, the MIP/ERGO/GCE electrode was incubated in PBS, containing 1 pM PROP for 1–10 min. The sensor response ($\Delta i/i_0\%$) measures the maximal value at 5 min and remains constant after that, indicating the equilibrium between the PROP molecules and the imprinted cavities has been reached. Thus, 5 min was considered the ideal time for conducting the rebinding process in subsequent experiments.

3.4 Analytical performance of the MIP/ERGO/GCE

At the optimal condition of the MIP sensor, Fig. 6a shows the DP voltammetric responses of MIP-ERGO/GCE after rebinding with PROP concentrations of 0.1 pM to 0.1 µM. The current of the redox probe decreases with increasing concentration, indicating the selective recognition to PROP molecules. The rebinding of PROP to the imprinted cavities reduces the number of sites available for the probe $[Fe(CN)_6]^{3-/4-}$ to reach the electrode surface. For comparison, the same procedure was carried out on NIP/ERGO/GCE (Fig. 6a, inset). An insignificant change in the electrode's response was measured. This is expected because the NIP is formed without adding of PROP template (i.e., no imprinted cavities). The calibration curve of the MIP sensor (Fig. 4b, curve a) revealed the proportionality of the sensor responses ($\Delta i/i_0\%$) with log PROP concentrations of 0.1 pM to 0.1 µM with a regression equation: $\Delta i/i_0\% = 623.05 + 46.55$ Log C [M] (R2 = 0.984). The responses recorded from NIP/ERGO/GCE after binding to PROP (0.1 pM to 0.1 µM) resulted in a fluctuated change with a regression equation of $(\Delta i/i_0\%) = 100.74 + 5.59$ Log C [M] (R2 = 0.739) of missed linear variation. Such results indicated the selective recognition of MIP/ERGO/GCE to PROP compared to NIP/ERGO/GCE (Fig. 6b, lines a & b). The sensor achieved a low detection limit of 0.08 pM as calculated from the relation of $3S_b/m$, where S is the standard deviation of the black response and m is the slope of the calibration curve [44].

The performance of the MIP/ERGO/GCE electrode was compared with other reported methods as shown in Table 1. Chromatographic-based approaches have been reported for PROP determination. The current MIP sensor is superior in terms of low limit of detection as well as the wider linear range. The presented method is the first developed electrochemical sensor for the determination of PROP at the trace level. The simplicity and selectivity are advantages of the technique. The low limit of detection obtained in this work is attributed to the combination of ERGO and MIP. ERGO increases electrode surface area and increases the number of imprinted cavities up to 15 times [31, 32]. With MIPs, the pre-concentration of the PROP to the MIP cavities improves the sensitivity. Low detection limits of 0.01 to 1 pM have been reported from electrochemical sensors based on nanomaterials MIP [32, 36].

3.5 Selectivity and repeatability studies

The ability of MIP-based sensors to discriminate the species of interest from interferants is crucial for their selectivity. The herbicide alachlor (ALA), fungicide carbendazim (CBZ), and the insecticide dimethoate (DMT) were utilized for MIP sensor selectivity evaluation. KCl and Na_2SO_4 were also tested. Three concentrations of 10 pM, 100 pM, and 1 nM were employed for each pesticide. The sensor responses measured from each interferent were compared to PROP (Fig. 7). The $\Delta i/i_0\%$ values for ALA, DMT, and CBZ are considerably lower than those obtained using PROP. At 100 pM, the sensor response for PROP was about 39-fold of ALA and nearly 17-fold to CBZ, and DMT, respectively; this confirms that the imprinted cavities preferentially

Table 1 Comparison of the proposed method with some reports for the PROP determination

Method	Linear range	Limit of detection	Sample	References
Gas chromatography (GC)-Mass Spectrometry	25–1000 µg/L	0.1 µg/kg	Soil	[14]
GC–mass spectrometry	0.05 to 1.0 mg/L	0.02 mg/kg	Rice, and soybean	[16]
Liquid chromatography based on supramolecular solvent microextraction	0.25 to 20 µg/g	0.07 µg/g	Soil	[20]
Solid-phase microextraction (SPME)-GC-electron capture detector (ECD)	0.5–500 µg/L	0.065 µg/L	Farm water	[17]
Full scan GC-mass spectrometry	0.05 mg/L to 20 mg/L	0.05 mg/ L	Atmospheric samples	[18]
LC–MS/MS and GC–MS/MS	2.5 pg/mg–100 pg/ mg	LOQ (2.5 pg/ mg	Hair of agricultural workers	[21]
QuEChERS citrate with GC–MS	0.01–0.50 mg/ kg	0.003 mg/ kg	Mango	[19]
Ultra-high-performance liquid chromatography- quadrupole time-of-flight mass spectrometry (UPLC-QTOF-MS)	0.25 to 100 µg/L	–	Tea	[22]
Voltammetric-based MIP (P*o*PD-PPy)-ERGO/GCE	21.1 pg/L–21.1 µg/L	16.9 pg/L	Water (tap & lake), red tea, and soil	The present work

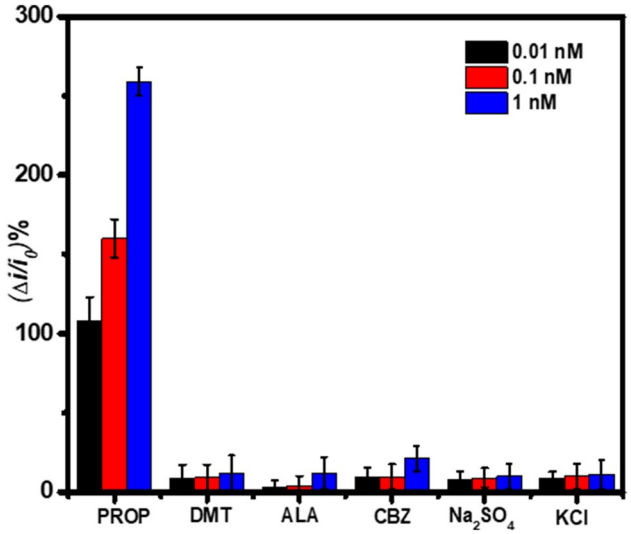

Fig. 7 MIP/ERGO/GCE sensor responses after the rebinding process for 5 min to PROP, ALA, CBZ, DMT (0.1 pM, 100 pM, 1 nM), and KCl and Na_2SO_4 (1 mM) in PBS, pH 7. The current response of the electrodes was monitored by DPV using a solution of 0.1 M KCl containing 2.0 mM $[Fe(CN)_6]^{3-/4-}$. The error bars represent the SD of three measurements

detected the PROP molecules among the compounds under investigation.

The difference in sensor values observed for CBZ and DMT is attributed to the relatively larger size of these molecules (compared to PROP molecules); this impedes their effective entry into the imprinted cavities due to steric hindrance. For ALA molecules, which are similar in size to PROP, the insignificant response indicates that the functional groups are also crucial for the selectivity of the MIP/ERGO/GCE electrode. The role of ions like K^+, Cl^-, Na^+, and SO_4^{2-} is also tested at 1.0 mM. Low sensor responses were measured after rebinding to 1.0 mM each. Such findings indicate an insignificant effect on the sensor selectivity. The results show that the proposed electrode is selective for determining PROP molecules.

The repeatability of the MIP sensor was evaluated by recording its responses five times after the rebinding process using a solution of 100 pM PROP. Following each measurement, the captured analyte was extracted by a methanol-acetic acid solution (9:1; v:v). The calculated RSD of 4.1% indicates acceptable sensor repeatability. The sensor reproducibility was also investigated using five different prepared sensors for the detection of 100 pM PROP. The RSD value of 6.4% demonstrated that the performance was good from one sensor to another.

3.6 Real sample application

Water samples (lake and tap), red tea, and soil were utilized to evaluate the efficiency of the proposed method. The PROP at various concentrations was added to each sample, and the MIP/ERGO/GCE sensor was used to determine the spiked PROP amounts. The recoveries were calculated based on the calibration curve. The results as found in Table 2 indicated the mean recoveries ranged from 95.24 to 111%, with relative standard deviations (RSDs) between 5.2 and 8.6%. Such findings refer to the sensor's good accuracy for PROP determination in environmental samples, and lake water.

4 Conclusions

We have developed the first molecularly imprinted poly (*o-PD*-co-Py) receptor for PROP's selective identification and determination based on an electrothermally reduced

Table 2 Recovery results for the detection of PROP using MIP sensor in water (lake and tap), red tea, and soil samples ($n = 3$)

Sample	Added (pM)	Detected (pM)	Recovery %	RSD %
Lake water	1	0.982	98.2	5.5
	10	11.1	111	6.3
	100	96.5	96.5	7.7
Tap water	1	0.978	97.8	5.8
	10	9.77	97.7	8.6
	100	106	106	7.3
Soil	1	1.12	112	5.2
	10	10.16	101.6	7.5
	100	95.24	95.24	8.1
Red tea	1	1.11	111	5.7
	10	10.24	102.4	6.1
	100	96.3	96.3	7.2

graphene oxide modified electrode. This low-cost and user-friendly sensor shows excellent analytical performance. The sensor's sensitivity is attributed to the high surface area of the ERGO-modified electrode and the selectivity from MIP film. The results demonstrated that the MIP/ERGO/GCE electrode exhibited good repeatability for the PROP electrochemical detection. The sensor showed a wide linear range for log PROP concentration (0.1 pM to 0.1 µM) with a low limit of detection of 0.08 pM. The MIP/ERGO/GCE electrode did not show significant interference of either structurally related or other pesticides, in addition to ions, demonstrating the sensor's good selectivity. The proposed sensor was successfully applied to water (lake and tap), red tea, and soil samples. Mean recoveries ranging from 95.24to 111% were obtained; this shows that the proposed sensor exhibits good accuracy in determining PROP in environmental samples.

Funding Open access funding provided by The Science, Technology & Innovation Funding Authority (STDF) in cooperation with The Egyptian Knowledge Bank (EKB).

Declarations

Conflict of interest The authors declare that they have no conflict of interest.

References

1. Postle JK et al (2004) Chloroacetanilide herbicide metabolites in Wisconsin groundwater: 2001 survey results. Environ Sci Technol 38(20):5339–5343. https://doi.org/10.1021/es040399h
2. Battaglin WA et al (2000) Occurrence of sulfonylurea, sulfonamide, imidazolinone, and other herbicides in rivers, reservoirs and ground water in the Midwestern United States, 1998. Sci Total Environ 248(2–3):123–133. https://doi.org/10.1016/s0048-9697(99)00536-7
3. Kolpin DW, Thurman EM, Linhart SM (2000) Finding minimal herbicide concentrations in ground water? Try looking for their degradates. Sci Total Environ 248(2–3):115–122. https://doi.org/10.1016/s0048-9697(99)00535-5
4. Liu C et al (2012) Dechlorinating transformation of propachlor through nucleophilic substitution by dithionite on the surface of alumina. J Soils Sediments 12(5):724–733. https://doi.org/10.1007/s11368-012-0506-0
5. Konstantinou I et al (2000) Removal of herbicides from aqueous solutions by adsorption on Al-pillared clays, Fe–Al pillared clays and mesoporous alumina aluminum phosphates. Water Res 34:3123–3136. https://doi.org/10.1016/S0043-1354(00)00071-3
6. Gençten M, Özcan A (2015) A detailed investigation on electro-Fenton treatment of propachlor: mineralization kinetic and degradation intermediates. Chemosphere 136:167–173. https://doi.org/10.1016/j.chemosphere.2015.04.101
7. Chemicals Known to the State to Cause Cancer or Reproductive Toxicity August 7, P.S.o.C.E.P.A. https://oehha.ca.gov/proposition-65/chemicals/propachlor
8. World Health Organization (1993) International programme on chemical, Propachlor. World Health Organization, Geneva
9. Dierickx PJ (1999) Glutathione-dependent cytotoxicity of the chloroacetanilide herbicides alachlor, metolachlor, and propachlor in rat and human hepatoma-derived cultured cells. Cell Biol Toxicol 15(5):325–332. https://doi.org/10.1023/A:1007619919336
10. Friedman CL, Lemley AT, Hay A (2006) Degradation of chloroacetanilide herbicides by anodic fenton treatment. J Agric Food Chem 54(7):2640–2651. https://doi.org/10.1021/jf0523317
11. Konstantinou IK, Sakkas VA, Albanis TA (2002) Photocatalytic degradation of propachlor in aqueous TiO2 suspensions. Determination of the reaction pathway and identification of intermediate products by various analytical methods. Water Res 36(11):2733–2742. https://doi.org/10.1016/S0043-1354(01)00505-X
12. Zheng W et al (2004) Transformation of herbicide propachlor by an agrochemical thiourea. Environ Sci Technol 38(24):6855–6860. https://doi.org/10.1021/es049384+
13. Qu JR et al (2012) Synthesis and utilisation of molecular imprinting polymer for clean-up of propachlor in food and environmental media. Food Chem 135(3):1148–1156. https://doi.org/10.1016/j.foodchem.2012.05.069
14. Sánchez-Brunete C, Albero B, Tadeo JL (2004) Multiresidue determination of pesticides in soil by gas chromatography−mass spectrometry detection. J Agric Food Chem 52(6):1445–1451. https://doi.org/10.1021/jf0354646
15. Raina R, Hall P (2008) Comparison of gas chromatography-mass spectrometry and gas chromatography-tandem mass spectrometry with electron ionization and negative-ion chemical ionization for analyses of pesticides at trace levels in atmospheric samples. Anal Chem Insights 3:111–125. https://doi.org/10.4137/aci.s1005

16. Wang L et al (2008) A rapid multi-residue determination method of herbicides in grain by GC-MS-SIM. J Chromatogr Sci 46(5):424–429. https://doi.org/10.1093/chromsci/46.5.424
17. Hwang YM, Wong YG, Ho WH (2005) Analysis of the chloroacetanilide herbicides in water using SPME with CAR/PDMS and GC/ECD. J AOAC Int 88(4):1236–1241
18. Borrás E et al (2011) Development of a gas chromatography-mass spectrometry method for the determination of pesticides in gaseous and particulate phases in the atmosphere. Anal Chim Acta 699(1):57–65. https://doi.org/10.1016/j.aca.2011.05.009
19. Martins FICC et al (2018) Method validation using normal and weighted linear regression models for quantification of pesticides in mango (*Mangifera indica* L.) samples. Chromatographia 81(4):677–688. https://doi.org/10.1007/s10337-018-3483-7
20. Dursun G, Yıldız E, Çabuk H (2018) Supramolecular solvent-based microextraction of propachlor and prometryn herbicides in soil samples prior to liquid chromatographic analysis. Cumhur Sci J. https://doi.org/10.17776/csj.452956
21. Park E et al (2021) Method for the simultaneous analysis of 300 pesticide residues in hair by LC-MS/MS and GC-MS/MS, and its application to biomonitoring of agricultural workers. Chemosphere 277:130215. https://doi.org/10.1016/j.chemosphere.2021.130215
22. Meng X et al (2022) Rapid determination of 134 pesticides in tea through multi-functional filter cleanup followed by UPLC-QTOF-MS. Food Chem 370:130846. https://doi.org/10.1016/j.foodchem.2021.130846
23. Akyüz D, Koca A (2019) An electrochemical sensor for the detection of pesticides based on the hybrid of manganese phthalocyanine and polyaniline. Sens Actuators B Chem 283:848–856. https://doi.org/10.1016/j.snb.2018.11.155
24. Elshafey R, Radi A-E (2018) Electrochemical impedance sensor for herbicide alachlor based on imprinted polymer receptor. J Electroanal Chem 813:171–177. https://doi.org/10.1016/j.jelechem.2018.02.036
25. Du H, Xie Y, Wang J (2021) Nanomaterial-sensors for herbicides detection using electrochemical techniques and prospect applications. TrAC Trends Anal Chem 135:116178. https://doi.org/10.1016/j.trac.2020.116178
26. El-Akaad S et al (2020) Capacitive sensor based on molecularly imprinted polymers for detection of the insecticide imidacloprid in water. Sci Rep 10(1):14479. https://doi.org/10.1038/s41598-020-71325-y
27. Yan C et al (2017) Electrochemical determination of enrofloxacin based on molecularly imprinted polymer via one-step electrocopolymerization of pyrrole and o-phenylenediamine. J Electroanal Chem 806:130–135. https://doi.org/10.1016/j.jelechem.2017.10.047
28. Yan C et al (2016) A selective strategy for determination of ascorbic acid based on molecular imprinted copolymer of o-phenylenediamine and pyrrole. J Electroanal Chem 780:276–281. https://doi.org/10.1016/j.jelechem.2016.09.046
29. Roushani M, Jalilian Z, Nezhadali A (2018) A novel electrochemical sensor based on electrode modified with gold nanoparticles and molecularly imprinted polymer for rapid determination of trazosin. Colloids Surf B 172:594–600. https://doi.org/10.1016/j.colsurfb.2018.09.015
30. Gui R, Guo H, Jin H (2019) Preparation and applications of electrochemical chemosensors based on carbon-nanomaterial-modified molecularly imprinted polymers. Nanoscale Adv 1(9):3325–3363. https://doi.org/10.1039/C9NA00455F
31. Beluomini MA et al (2019) Electrochemical sensors based on molecularly imprinted polymer on nanostructured carbon materials: a review. J Electroanal Chem 840:343–366. https://doi.org/10.1016/j.jelechem.2019.04.005
32. Beluomini MA et al (2017) D-mannitol sensor based on molecularly imprinted polymer on electrode modified with reduced graphene oxide decorated with gold nanoparticles. Talanta 165:231–239. https://doi.org/10.1016/j.talanta.2016.12.040
33. Qian L et al (2021) Graphene oxide-based nanomaterials for the electrochemical sensing of isoniazid. ACS Applied Nano Materials 4(4):3696–3706. https://doi.org/10.1021/acsanm.1c00178
34. Qian L et al (2020) Graphene-oxide-based electrochemical sensors for the sensitive detection of pharmaceutical drug naproxen. Sensors (Basel, Switzerland) 20(5):1252. https://doi.org/10.3390/s20051252
35. Roy S et al (2011) Graphene oxide for electrochemical sensing applications. J Mater Chem 21(38):14725–14731. https://doi.org/10.1039/C1JM12028J
36. Pompeu Prado Moreira LF, Buffon E, Stradiotto NR (2020) Electrochemical sensor based on reduced graphene oxide and molecularly imprinted polyphenol for d-xylose determination. Talanta 208:120379. https://doi.org/10.1016/j.talanta.2019.120379
37. Essousi H et al (2020) An electrochemical sensor based on reduced graphene oxide, gold nanoparticles and molecular imprinted over-oxidized polypyrrole for amoxicillin determination. Electroanalysis 32(7):1546–1558. https://doi.org/10.1002/elan.201900751
38. Pereira TC, Stradiotto NR (2019) Electrochemical sensing of lactate by using an electrode modified with molecularly imprinted polymers, reduced graphene oxide and gold nanoparticles. Microchim Acta 186(12):764. https://doi.org/10.1007/s00604-019-3898-3
39. Elshafey R, Abo-Sobehy GF, Radi A-E (2021) Imprinted polypyrrole recognition film @cobalt oxide/electrochemically reduced graphene oxide nanocomposite for carbendazim sensing. J Appl Electrochem. https://doi.org/10.1007/s10800-021-01613-6
40. Marcano DC et al (2010) Improved synthesis of graphene oxide. ACS Nano 4(8):4806–4814. https://doi.org/10.1021/nn1006368
41. Boukamp BA (1986) A nonlinear least squares fit procedure for analysis of immittance data of electrochemical systems. Solid State Ionics 20(1):31–44. https://doi.org/10.1016/0167-2738(86)90031-7
42. Meland AK, Bedeaux D, Kjelstrup S (2005) A Gerischer phase element in the impedance diagram of the polymer electrolyte membrane fuel cell anode. J Phys Chem B 109(45):21380–21388. https://doi.org/10.1021/jp050635q
43. Lorenzo RA et al (2011) To remove or not to remove? the challenge of extracting the template to make the cavities available in Molecularly Imprinted Polymers (MIPs). Int J Mol Sci 12(7):4327–4347
44. Long GL, Winefordner JD (1983) Limit of detection a closer look at the IUPAC definition. Anal Chem 55(07):712A-724A. https://doi.org/10.1021/ac00258a724